UC San Diego
UC San Diego Previously Published Works

Title
Preventive Inhibition of Liver Tumorigenesis by Systemic Activation of Innate Immune Functions

Permalink
https://escholarship.org/uc/item/15w0d7wh

Journal
Cell Reports, 21(7)

ISSN
2639-1856

Authors
Lee, Jin
Liao, Rui
Wang, Gaowei
et al.

Publication Date
2017-11-01

DOI
10.1016/j.celrep.2017.10.064

Peer reviewed

Preventive Inhibition of Liver Tumorigenesis by Systemic Activation of Innate Immune Functions

Jin Lee[1], **Rui Liao**[1,4], **Gaowei Wang**[1], **Bi-Huei Yang**[5], **Xiaolin Luo**[1], **Nissi M. Varki**[1], **Shuang-Jian Qiu**[4], **Bing Ren**[6], **Wenxian Fu**[5], and **Gen-Sheng Feng**[1,2,3,7,*]

[1]Department of Pathology, School of Medicine, University of California San Diego, La Jolla, California, USA 92093

[2]Molecular Biology Section, Division of Biological Sciences, University of California San Diego, La Jolla, California, USA 92093

[3]Moores Cancer Center, University of California San Diego, La Jolla, California, USA 92093

[4]Liver Cancer Institute, Zhongshan Hospital, Fudan University, Shanghai 200032, China

[5]Pediatric Diabetes Research Center, Department of Pediatrics and Institute for Diabetes and Metabolic Health, University of California San Diego, La Jolla, CA, 92093-0983

[6]Ludwig Cancer Research Institute, Department of Cellular and Molecular Medicine, University of California San Diego, La Jolla, CA, 92093

Summary

Liver cancer has become the second most deadly malignant disease, with no efficient targeted or immune therapeutics available yet. In dissecting roles of cytoplasmic signaling molecules in hepatocarcinogenesis using an inducible mouse gene targeting system, *Mx1-cre,* we identified a potent liver tumor-inhibitory effect of synthetic double-stranded RNA (dsRNA), polyinosinic-polycytidylic acid (pIC), an inducer of the *Mx1-cre* system. Injection of pIC at the pre-cancer stage robustly suppressed liver tumorigenesis either induced by chemical carcinogen or by Pten loss and associated hepatosteatosis. The immunostimulatory dsRNA inhibited liver cancer initiation, apparently by boosting multiple anti-tumor activities of innate immunity, including

[*]Correspondence should be addressed to: Gen-Sheng Feng, gfeng@ucsd.edu.
[7]Lead Contact

induction of immunoregulatory cytokines, activation of NK cells and dendritic cells, and reprogramming macrophage polarization. This study paves a way for development of preventive and early interfering strategies for liver cancer, to reduce the rapidly increasing incidences of liver cancer in an ever-growing population with chronic liver disorders.

Graphical Abstract
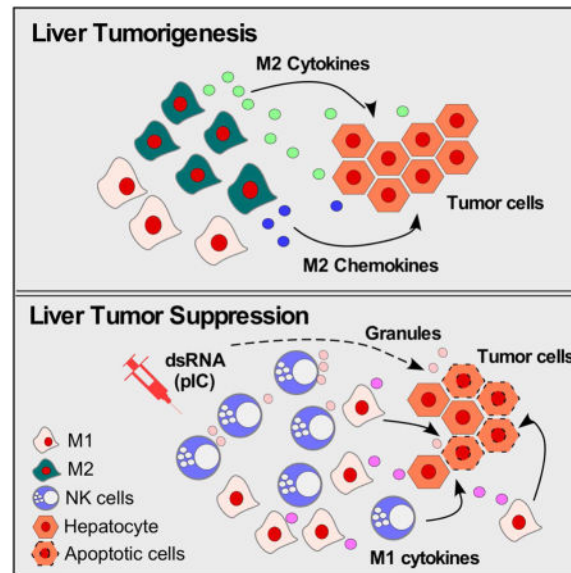
INTRODUCTION

In contrast to overall cancer statistics, primary liver cancer, in particular hepatocellular carcinoma, is increasing in incidence and mortality worldwide (Ryerson et al., 2016). In fact, liver cancer has become the second most deadly malignant disease worldwide (Llovet et al., 2016), in part due to the rise of metabolic disorders, including alcoholic and non-alcoholic fatty liver diseases, and viral hepatitis (Farazi and DePinho, 2006; Michelotti et al., 2013). Unfortunately, the rapid increase of this malignant disease has not been met by effective therapeutics in the clinic. Surgical resection and liver transplantation remain the primary options for liver cancer patients (Poon, 2011).

Development of effective therapeutic strategies relies on in-depth analysis of the molecular and cellular mechanisms that drive liver tumorigenesis. Parallel with genomic screening of mutations in human patients' specimens (Zucman-Rossi et al., 2015), characterization of cell type-specific gene knockout mouse models has demonstrated, ironically, anti-oncogenic effects of classical oncoproteins (Feng, 2012). Deletion of c-Met, EGFR, β-catenin, Akt, Ikkβ, Jnk, and Shp2 in hepatocytes astonishingly led to exacerbated HCC development induced by the chemical carcinogen diethylnitrosamine (DEN) (Feng, 2012; Lanaya et al., 2014; Wang et al., 2016), disclosing previously unrecognized complexity in hepato-oncogenesis. Several groups have dissected the underlying mechanisms, using mouse lines with genetic ablation in different hepatic cell types (Das et al., 2011; Lanaya et al., 2014; Maeda et al., 2005). Although *Albumin-cre*-mediated deletion of *Ikkβ, Jnk1/2,* or *EGFR* in

hepatocytes aggravated DEN-induced HCC, *Mx1-cre*–driven removal of any of these genes in both hepatocytes and non-parenchymal cells (NPCs) resulted in tumor suppression. These opposing effects led to a proposal that disruption of an inflammatory cytokine circuit, i.e. interleukin 1α (IL-1α)-induced IL-6 production by Kupffer cells, inhibits hepatocarcinogenesis (Das et al., 2011; Lanaya et al., 2014; Maeda et al., 2005).

Similarly, we previously identified HCC-promoting effects of *Ptpn11/Shp2* deficiency, by ablating the gene in hepatocytes using the *Albumin-cre* system (Bard-Chapeau et al., 2011). In this current study, further analysis of *Ptpn11/Shp2* deletion in hepatocytes and NPCs using the *Mx1-cre* system have fortuitously led to identification of a potent inhibitory effect on liver cancer initiation by a synthetic double-stranded RNA (dsRNA), polyinosinic-polycytidylic acid (pIC), the inducer of the *Mx1-cre* system. pIC structurally mimics dsRNAs and potently activates pattern recognition receptors Toll-like receptor 3 (TLR3), retinoic acid-inducible gene I (RIG-I)/melanoma differentiation-associated protein 5 (MDA5) and dsRNA-activated protein kinase (PKR) (Barton and Medzhitov, 2003). Extensive molecular and immunological analyses suggest that pIC suppresses initiation of liver tumorigenesis, likely by reprogramming macrophage polarization and activating natural killer (NK) cells and dendritic cells. Given the extremely poor prognosis of liver cancer patients diagnosed at advanced stages, this study demonstrates the feasibility of a new preventive strategy for liver cancer, which may benefit a rapidly expanding population of at-risk patients with various chronic liver diseases.

RESULTS

Injection of pIC suppresses chemically-induced HCC development

We demonstrated previously that *Alb-cre*–mediated deletion of *Shp2/Ptpn11* in hepatocytes (*Shp2^{F/F}:Alb-cre; Shp2^H*) enhanced DEN-induced HCC (Bard-Chapeau et al., 2011), similar to the tumor-promoting effect of ablating Ikkβ, Jnk or EGFR in hepatocytes. In this study, we further dissected the role of Shp2 in liver tumorigenesis in distinct inducible gene deletion mouse line (*Shp2^{F/F}:Mx1-cre; Shp2^{iL}*), by breeding *Shp2^{F/F}* mouse with *Mx1-cre* transgenic mouse. Of note, while the *Albumin* promoter is spontaneously active in hepatocytes, *Mx1 (myxovirus resistance I)* is responsive to the interferons (IFN) induced by pIC (Kuhn et al., 1995). As shown in Figure 1A, Shp2 was deleted in hepatocytes in *Shp2^H* mice, and was deleted in both hepatocytes and macrophages (Kupffer cells) in *Shp2^{iL}* livers, following pIC injection. Compared to *Shp2^H* livers, Shp2 protein was not detectable in *Shp2^{iL}* liver lysates (Figure S1A), indicating a more broad deletion of Shp2 in hepatocytes and NPCs in the liver.

To determine the impact of Shp2 deletion on HCC in *Shp2^{iL}* mice, we injected pIC intraperitoneally (i.p.) on postnatal day 9, 11, and 13 (D9, 11, 13), followed by DEN injection on D15 (Figure 1B), using a published protocol (Lanaya et al., 2014; Maeda et al., 2005). As liver tumorigenesis is highly associated with inflammation, one concern was that an inflammatory milieu elicited by pIC could confound the interpretation of the experiment. To parse a possible effect of pIC itself on tumorigenesis, we divided the *WT* control (*Shp2^{F/F}*), *Shp2^H*, and *Shp2^{iL}* mice into two subgroups, and injected the same dosage of pIC into one subgroup of all three genotypes (Figure 1B). All animals were then examined

for tumor burdens at 8 months, by evaluating maximal tumor sizes, numbers, and the liver/ body weight ratios. We observed DEN-induced tumor nodules in all three genotypes of animals, with the most severe tumor lesions observed in $Shp2^{H}$ livers (Figure 1C), consistent with previous results (Bard-Chapeau et al., 2011). Histological analysis identified HCC as the major tumor type (Figure 1C), positive for α-fetoprotein (AFP) expression (Figure S1B). The pIC administration modestly suppressed DEN-induced tumorigenesis in $Shp2^{iL}$ mice, and also in the $WT(Shp2^{F/F})$ animals (Figure 1C–F). Interestingly, pIC treatment exhibited the most robust inhibitory effect on tumor growth in $Shp2^{H}$ mice (Figure 1C–F), despite the dsRNA injection rendering no impact on Alb-cre-mediated gene deletion (Figure S1C). Immunostaining of liver sections detected markedly decreased PCNA^{+} cells in tumors in pIC-treated $Shp2^{H}$ livers (Figure S1D). pIC treatment also increased the expression of TLR3 and MAVS in surrounding non-tumor areas (Figure S1B). Together, these results indicate a tumor-inhibitory effect of pIC in all three genotypes of mice, unrelated to its induction of gene deletion.

pIC has a robust HCC-inhibiting effect if given at the pre-cancer stage

The results described above indicate a potent anti-oncogenic effect of pIC independent of its induction of gene ablation. In subsequent experiments, we focused on $Shp2^{H}$ mice, as pIC injection induced the strongest tumor-inhibitory effect without affecting gene deletion mediated by Alb-cre in this mouse line. Further, the $Shp2^{H}$ mutant mice developed hepatic inflammation, cholestasis and fibrosis, mimicking pathogenic processes in human patients with chronic liver diseases predisposed to tumorigenesis (Bard-Chapeau et al., 2011; Li et al., 2014).

We injected 3 doses of pIC into $Shp2^{H}$ mice at different time points, starting at D9, or at 1, 3 or 5 months of age (Figure 2A). All animals received DEN at D15, and tumor loads were examined at 8 months. The most robust decrease of tumor numbers, sizes and liver/body weight ratios was detected when pIC was administered at D9 or at 1 month (Figure 2B–E). pIC given at 3 months had less but still significant inhibition on tumor numbers and sizes, although the liver/body weight ratios were not changed significantly (Figure 2C). Injection of the same pIC dosage at 5 months, after DEN-induced tumor initiation (He et al., 2010), had very minor impact on tumor loads, compared to controls (Figure 2B–E). Although this experiment did not rule out a possible role of pIC in suppressing tumor progression at the early stage, it suggests a potent effect of pIC in preventing HCC initiation,

pIC reprograms liver macrophages during liver tumorigenesis

To probe the mechanisms of the tumor-inhibitory effect of pIC, we examined intrahepatic immune cell infiltration in DEN-induced tumor-bearing mice. We analyzed the proportions and abundance of major immune cell populations, including CD4^{+} T cells (CD4^{+}Foxp3^{-}), CD8^{+} T cells (NK1.1^{-}CD4^{-}), regulatory T (Treg) cells (CD4^{+}Foxp3^{+}), NK cells (NK1.1^{+}), NKT cells (NK1.1^{+}TCRβ^{+}), macrophages (CD11b^{+}F4/80^{+}) and dendritic cells (CD11c^{+}). No significant differences were detected between control and pIC-treated mice for populations of CD4^{+}, CD8^{+} T cells, dendritic cells and macrophages in the tumor-bearing livers (Figure S2A–F). Since inflammation is a critical factor in HCC development, we performed more detailed analysis of infiltrating hepatic macrophages. The classically

activated M1 macrophages are known to mediate inflammatory response, pathogen clearance, and anti-tumor immunity, while the alternatively activated M2 macrophages exert a tumor-promoting effect (Mills, 2012). Immunostaining detected dramatically increased infiltration of F4/80^{+} cells in *Shp2* [H] mice compared to *Shp2F/F* mice (Figure S2G–H). In the liver of DEN-treated *Shp2* [H] mice, we detected marked increase in CD163-positive cells, suggesting a skewing toward M2 macrophage phenotype bias (Figure S2G, I). In contrast, the expression of CD163 was significantly reduced in pIC-treated *Shp2* [H] mice (Figure S2G, I), suggesting an inhibitory effect of pIC on macrophage polarization into an M2 phenotype in the tumor microenvironment. Consistent to this notion, we observed that pIC significantly suppressed production of M2 cytokines, such as CCL17, CCL22 and IL-4, while increasing the expression of a pro-inflammatory cytokine IP-10 (Figure S2J–N).

The increased abundance of M2 macrophages in the liver correlated with severity of tumor growth in *Shp2* [H] mice. We then asked if this abnormal accumulation of M2 macrophages resulted from altered skewing of M1 to M2 macrophages during tumor progression in *Shp2* [H] mice, and whether pIC treatment had any impact on the shift towards M1 polarization. As DEN injection on day 15 induced tumor initiation within 5 months (He et al., 2010), we measured the expression of M1- or M2-related cytokines and chemokines at 1, 3 and 5 months. Expression of CCL17 and CCL22 was markedly increased in *Shp2* [H] mice, at 3 and 5 months (Figure 2F). pIC treatment significantly suppressed expression of CCL17 and CCL22 in *Shp2* [H] mice examined at 3 months (Figure 2G). Consistent with this observation, immunostaining showed reduced F4/80[+] areas and decreased expression of CD163 at 3 months following pIC treatment (Figure 2H–I). Thus, pIC treatment promoted M1 macrophage development at the expense of tumor-promoting M2 macrophages during the pre-cancer stage.

dsRNA suppresses liver tumorigenesis driven by Pten loss and hepatosteatosis

The above-described results define a potent tumor-inhibitory role of pIC in a DEN-induced HCC model. To expand on this observation, we further investigated its effect on liver tumorigenesis induced by deletion of Pten, a tumor suppressor frequently mutated or lost in liver and other types of cancer (Song et al., 2012; Worby and Dixon, 2014). Several groups showed that *Alb-cre*-mediated deletion of Pten (*Pten* [H]) caused severe non-alcoholic fatty liver disease (NAFLD) followed by development of HCC and ICC (intrahepatic cholangiocarcinoma) spontaneously, without DEN treatment (Galicia et al., 2010; Horie et al., 2004). We injected pIC into *Pten* [H] mice (Figure 3A, B) on D9, and tumor loads were examined at 9 months. pIC treatment significantly reduced tumor numbers, maximal tumor sizes and the liver/body weight ratios (Figure 3C–F), suggesting pIC has a similar tumor-suppressing effect in liver tumorigenesis driven by Pten deficiency.

In accordance with previous report (Horie et al., 2004), we found that Pten removal from hepatocytes induced severe hepatosteatosis in mice. Interestingly, Oil-red-o staining indicated that pIC treatment had no effect on the fatty liver phenotype in *Pten* [H] mice (Figure 3G). pIC also did not significantly change the expression of lipogenic transcription factors or enzymes (Xu et al., 2013), including sterol regulatory element binding protein-1c (SREBP-1c), carbohydrate-responsive element-binding protein (ChREBP), fatty acid

synthase (FAS) and Acetyl-CoA carboxylase 1 (ACC1) (Figure 3J). However, pIC administration significantly reduced the number of F4/80-positive cells in the liver (Figure 3G, I), and the expression of CCL17, compared to the control group (Figure 3J). We examined intrahepatic immune cell subsets in *Pten* [H] mice, and detected decreased numbers of CD4$^+$ T cells and NKT cells in pIC-treated livers (Figure S3A–E), consistent with a previous report on complicated roles of NKT and CD8 T cells in NASH-driven HCC (Wolf et al., 2014). Therefore, pIC treatment inhibited tumorigenesis induced by Pten loss, without impact on the associated hepatosteatosis.

Transcriptomic analysis of pIC-treated livers

To extensively investigate the mechanisms of the pIC anti-tumor effect, we performed RNA-sequencing (RNA-seq) analysis of RNAs isolated from liver tissues at 1 and 2 weeks after pIC injection into DEN-treated *Shp2* [H] mice. Differentially expressed genes were identified by a cut-off of 2-fold and q-values of <0.05. As shown in Figure S4A, more genes were affected by pIC treatment at 2 weeks (1246) than 1 week (750) (Figure 4A). By combining the 1- and 2-week data, we found that 469 genes were affected at both time points (Figure 4A), and as highlighted on the heatmap, these genes are mainly involved in immune responses (Figure 4B). Gene set enrichment analysis (GSEA) of the commonly up- and down-regulated genes demonstrated that the hepatic response to pIC treatment was mainly associated with the immune system (Figure 4B). Ingenuity pathway analysis (IPA) also suggested markedly increased leukocyte movement and infiltration in pIC-treated *Shp2* [H] livers (Figure 4C). Canonical pathways in immune response analyzed by IPA identified dendritic cell maturation, role of pattern recognition receptors in recognition of bacteria and viruses, and production of NO and ROS species in macrophages (Figure 4D). Of note, pIC treatment potently induced up-regulation of inflammatory genes, including IFNγ, STAT1, TLR4 and TNF, in *Shp2* [H] livers (Figure 4E). Together, these results suggest that pIC treatment elicits the activation of multiple inflammatory pathways, which favors an anti-tumor microenvironment in the DEN-induced HCC model.

We performed similar transcriptomic analysis in *Pten* [H] livers at 1 and 2 weeks after pIC treatment (Figure 4F, Figure S4B). In total, 91 genes were commonly affected by pIC at these two time points in *Pten* [H] livers. Functional annotation revealed that these genes were distinct from those affected by pIC in *Shp2* [H] livers (Figure 4F–H). IPA analysis identified top pathways enriched in liver necrosis/cell death and impaired tumor growth (Figure 4H, I). pIC treatment induced potently signature genes corresponding to PTGER2, EP400, MED1 and STAT3 in *Pten* [H] livers (Figure 4J). Genes with changed expression of less than 2-fold (but with significant *q* value) were mostly enriched in immune responses pathways (Figure S4C).

Although pIC exhibited similar anti-oncogenic effects in the two mouse tumor models, RNA-seq analysis revealed differential gene sets affected by the dsRNA in *Shp2* [H] and *Pten* [H] livers. To explore a common mechanism for pIC-induced responses, we searched for genes that were changed in both *Shp2* [H] and *Pten* [H] mice at the two time points. In total, we identified 44 genes up-regulated and 17 genes down-regulated at 1 week in both mouse lines (Figure S4D), and only 9 genes up-regulated and 14 genes down-regulated at 2 weeks after

pIC treatment (Figure S4D). Gene ontology enrichment identified the shared gene-set at 1 week highly enriched in immune regulation. Using ingenuity IPA analysis, we inferred master regulators for downstream targets based on these commonly affected genes in both *Shp2* ^{H} and *Pten* ^{H} mice. Pathways regulated by FcεR1G, IRF3, IFNβ, C/EBPα and STAT1 were clearly activated (Figure S4G). We then performed further analysis of the RNA-seq data using Cybersort software to investigate the effect of pIC treatment on cell subsets in *Shp2* ^{H} and *Pten* ^{H} livers. The data consistently showed increase of type 1 macrophages and decrease of resting NK cells in the pIC-treated groups (Figure S4H–I). These results clearly highlight the activation of the TLR3 pathway by pIC and subsequent activation of IRF3, resulting in enhanced type 1 IFN and STAT1 signaling. We also analyzed genes that were distinctly changed in *Shp2* ^{H} and *Pten* ^{H} livers, at 1 and 2 weeks after pIC treatment (Figure S4G). IPA analysis of the divergent gene-sets at 1 and 2 weeks showed LPS/IL-1 inhibition-mediated RXR function, nicotine degradation, and melatonin degradation among others (Figure S4J–Q).

pIC activates multiple innate immune functions to inhibit liver tumorigenesis

To support the RNA-seq data and also to identify the cellular participants in pIC-mediated HCC suppression, we performed flow cytometric analysis to dissect the alterations in immune cell subpopulations in *Pten* ^{H} and DEN-treated *Shp2* ^{H} livers 1 week after pIC injection (Figure S5). We observed a significant increase in several innate immune cell populations including dendritic cells, macrophages and NK cells in pIC-treated *Shp2* ^{H} and *Pten* ^{H} livers (Figure 5A–B). In contrast, the abundance of CD4$^+$ and CD8$^+$ T cells were unaffected or even reduced (Figure 5A–B). More detailed flow cytometric analysis showed that pIC treatment increased NK cells and macrophages in *Shp2* ^{H} and *Pten* ^{H} livers (Figure 5C–F), Consistent with the flow cytometric data, immunostaining detected aggregation of F4/80$^+$ macrophages in pIC-treated livers, relative to controls (Figure 5G–H). We performed further characterization of the F4/80^{hi} population to examine various macrophage subpopulations, as described previously (Wang and Kubes, 2016). pIC injection rapidly increased expression of CD102 and MHCII, markers for M1 and peritoneal macrophages, without impact on expression of CD206 (M2 marker), in gated F4/80^{hi} cell population (Figure S5). Immunostaining also demonstrated that pIC treatment induced significant increase of M1 macrophages (iNOS$^+$), accompanied by decrease of M2 macrophages (CD163$^+$) (Figure S6A). qRT-PCR analysis confirmed elevated expression of M1-related genes, including CXCL2, CCR8, CXCR2 and NOS2, and impaired expression of M2-related genes such as Retnla and Arg1 in pIC-treated *Shp2* ^{H} and *Pten* ^{H} livers, relative to controls (Figure S6B). Further, RNA-seq analysis identified an immunological signature gene set among pIC-responsive genes in *Shp2* ^{H} and *Pten* ^{H} livers, which are mainly involved in monocyte/macrophage differentiation and NK cell activation (Figure 5I, J). Thus, pIC treatment boosted innate immunity and fostered an anti-tumor microenvironment in the liver.

Consistent with the RNA-seq data (Figure 4B), pIC treatment upregulated TLR3 expression, p-p38 MAP kinase, and p-Stat1 levels in *Shp2* ^{H} and *Pten* ^{H} liver lysates (Figure 6A). Perforin, a protein in secreting granules from NK and CTL cells, was increased by pIC in *Shp2* ^{H} and *Pten* ^{H} livers (Figure 6B). Also upregulated by pIC in the two mutant livers was TNFSF10 (Figure S4G), which acts as a pro-apoptotic molecule to activate caspase-8 and

subsequently caspase-3. Indeed, pIC treatment induced production of cleaved caspase 3 and Bax protein, accompanied by decreased expression of Bid, in *Pten* [H] and DEN-treated *Shp2* [H] livers (Figure 6B). We detected significantly more dying hepatocytes in *Pten* [H] and DEN-treated *Shp2* [H] liver sections following pIC injection (Figure 6C–E), and TUNEL^{+} cells were mostly localized in areas around portal vein (Figure 6C). However, no significant impact on hepatocyte death was observed in *WT* livers following pIC injection (Figure S7C).

We injected clodronate liposomes to deplete macrophages or anti-NK1.1 antibody to deplete NK cells 24 hrs before pIC treatment. Interestingly, efficient depletion of macrophages, as verified by F4/80 staining, resulted in dramatic suppression of hepatocyte death in *Pten* [H] and DEN-treated *Shp2* [H] livers (Figure 6C–E). Similarly, depleting NK cells abolished pIC-induced increase of cell death in DEN-treated *Shp2* [H] livers (Figure S7A–B), suggesting that both macrophages and NK cells are likely involved in pIC-induced cell death in both models. Furthermore, we examined p21 and SA-β-gal levels, and detected significantly enhanced cellular senescence in pIC-treated *Shp2* [H] and *Pten* [H] livers, relative to controls (Figure S7D–F), and qRT-PCR analysis also detected significantly increased expression of *p16, p21* and *p53*, genes involved in cell senescence (Figure S7G).

The results in Figure 2 suggest a more potent inhibition of pIC on HCC initiation than progression in mice, as maximal effect was observed if injected at the pre-cancer stage. Therefore, we suspected a possible role of pIC in inhibiting genesis or expansion of liver tumor-initiating cells (TICs). Immunostaining demonstrated significant decrease of CD44v6[+], SOX9^{+}, EpCam[+] and V6[+] cell numbers in *Pten* [H] and DEN-treated *Shp2* [H] liver sections 7 days following pIC treatment (Figure S7H–L). These markers have been previously shown to be associated with liver TICs by a number of groups (Liu et al., 2016; Luo et al., 2016; Yamashita and Wang, 2013). Of note, pIC injection did not cause severe hepatotoxicity, as reflected by serum ALT levels (Figure S7M). In aggregate, the inhibitory effect of pIC on liver tumorigenesis is likely through multiple mechanisms involving enhanced innate immunity, elevated cell senescence and death, and impaired TIC expansion (Figure 7).

DISCUSSION

In contrast to the current prevailing enthusiasm for precision or personalized medicine (Friedman et al., 2015; Vargas and Harris, 2016), our studies document a potential universal approach to cancer immune therapy. We present evidence that a non-specific immunostimulatory dsRNA, a well-known experimental reagent, has a broad and powerful anti-tumor effects in two different animal models of liver cancer. We identified this potent liver tumor-inhibitory activity unexpectedly in experiments originally designed to examine the effect on HCC development of pIC-induced and *Mx1-cre*-mediated gene deletion in hepatocytes and NPCs (Figure 1). The *Mx1-cre* system is the first established inducible gene deletion approach in mice (Kuhn et al., 1995). This is still a most widely used conditional gene targeting method, with the premise that injecting pIC into mice may only exert transient molecular and physiological effects. However, the additional stringent controls used in this study reveal a robust cancer-inhibiting effect even eight months after pIC

injection. This data underscores the need for added caution in data interpretation, especially in research of liver cancer, which is highly associated with inflammation during pathogenesis. Of note, this tumor-inhibitory effect of pIC was detected by several other groups in previous studies on Ikkβ, Jnk1/2 and EGFR in liver tumorigenesis (Das et al., 2011; Lanaya et al., 2014; Maeda et al., 2005). However, the effect was attributed to the target gene deletion in different hepatic cell populations, and disruption of an IL-1α-IL-6 cytokine communication circuit between hepatocytes and Kupffer cells. Our data presented here provide unequivocal evidence that it is pIC, the inducer of the inducible gene deletion system, that possesses this robust anti-tumor activity in the liver, independent of its intended role in the inducible gene deletion system.

By injecting pIC at different time points, we observed its most potent tumor-inhibitory effect when administered in the pre-cancer stages, suggesting a more prominent preventive than therapeutic role in liver cancer. Consistent with this observation, we identified significantly reduced expression of biomarkers, such as CD44v6, Sox9, A6 and EpCAM, immediately following pIC injection (Figure S7). The increased expression of these biomarker molecules was arguably associated with genesis of liver TICs in various animal models, and pIC-induced downregulation of their expression correlated with suppression of liver tumorigenesis in this study. It is remarkable that pIC injection also suppressed liver tumorigenesis driven by Pten loss and hepatic steatosis without inhibiting steatosis (Figure 3). These data provide a proof of principle for use of non-specific immune-stimulators, such as synthetic dsRNA, to prevent HCC development in high risk patients with fatty liver disease. Non-targeted immunomodulators such as imiquimod, resiquimod, and Bacillus-Calmette-Guerin (BCG) have been approved by the FDA for use in prevention of basal cell carcinoma and bladder cancer (Brausi et al., 2011; Narayan et al., 2012). The significance for development of an effective prevention strategy for liver cancer cannot be over-emphasized, given the extremely poor prognosis of liver cancer patients at the advanced stages and the rapidly expanding population of patients with chronic liver diseases, who are at high risk for liver tumorigenesis,

We have extensively analyzed the underlying mechanisms of the pIC tumor-suppressing effect in two animal models of liver cancer. The results presented above suggest that the synthetic dsRNA potently stimulated many functions of innate anti-tumor immunity, especially activation of NK cells, M1 macrophages, and dendritic cells in the liver. Accumulation of M2 macrophages in the tumor microenvironment was found to correlate with the tumor burden in DEN-treated $Shp2^H$ mice, with or without pIC injection (Figure 2; Figure S2). We found that pIC treatment reprogrammed macrophages, increasing M1 and decreasing M2 cells during the pathogenic process (Figure 2; Figure S2). To extend these observations, we determined the immediate effects of pIC by analyzing the M1 and M2 markers in liver tissues one week after its injection. Indeed, pIC induced upregulation of M1 and downregulation of M2 macrophage markers (Figure 5, Figure S5, Figure S6). Another notable effect is acute NK cell activation and expansion by pIC in both $Shp2^H$ and $Pten^H$ livers (Figure 5, Figure S7). We further identified that pIC treatment resulted in significant increase of hepatocyte death in livers injured by DEN injection or by Pten loss, and the pIC-mediated effect was inhibited following depletion of macrophages or NK cells (Figure 6, Figure S7). Together, these results suggest a model (Figure 7), in which pIC injection

triggered multiple functions of innate immunity, in particular activation of NK and M1 macrophages, which may be involved in clearance of "high risk" cancerous cells at the pre-cancer stage, resulting in preventive suppression of liver tumorigenesis. More definitive functional analysis is warranted to test this model and to define the roles of these cell populations in the observed anti-tumor immunity.

Although we did not observe therapeutic inhibition of tumor progression when pIC was administered after tumor initiation (at age of 5 months), this was tested with only 3 injections, following a protocol not designed for therapeutic purpose. It is conceivable that adjusting the injection times and dosages may achieve a suppressing effect of pIC on HCC progression. pIC injection also induced a milieu of cytokines that can modulate adaptive immunity and T and B lymphocyte functions. Furthermore, despite its immuno-stimulatory activity, RNA-seq data showed that pIC treatment also upregulated CD279 (PD-L1) expression, an immuno-suppressing molecule of T cells (Zou et al., 2016). Thus, combined administration of pIC with antibodies against immune-inhibitory molecules, such as PD-L1, may achieve effective therapeutic results in HCC patients at advanced stages, and pIC may be used as an immune adjuvant to boost anti-tumor immunity in liver cancer therapy.

METHODS

Mice

All mouse lines in this study were in C57BL/6 background. All animal experimental protocols (S09108) have been approved by the University of California San Diego Animal Care Program following National Institutes of Health Guidelines. Generation of $Shp2^{H}$ ($Shp2^{F/F}$:Alb-cre), $Shp2^{iL}$ ($Shp2^{F/F}$:Mx1-cre), and $Pten^{H}$ ($Pten^{F/F}$:Alb-cre) was described previously (Bard-Chapeau et al., 2011; Galicia et al., 2010; Zhu et al., 2011). Male mice were used to monitor HCC development.

Tumor induction and analysis

For the DEN-induced HCC model (Figure 1b), all three groups of mice were fed a commercial diet and water *ad libitum*. Mice were intraperitoneally (IP) injected with 25 mg/kg of DEN (N0258-1G; Sigma-Aldrich) on day 15 (D15), and received three consecutive injections of pIC (15 μg/g, GE healthcare) on D9, 11 and 13, as described previously (Bard-Chapeau et al., 2011; Maeda et al., 2005). In experiments described in Figure 2A, male mice received pIC at 1, 3 or 5 months of age, with 3 IP injections every other day. Tumor loads were examined at 8 months (Figure 2A). All male mice were sacrificed between 3:00 and 5:00 p.m. during the day, to minimize circadian effect on variations of gene expression and liver physiology. Externally visible tumors (0.5 mm) were counted and measured by stereomicroscopy. Large lobes were fixed in z-Fix overnight and paraffin embedded sections were processed for H&E staining. Remaining lobes were microdissected into tumors and non-tumor tissues and stored at −80 °C until analysis.

Histology, immunohistochemistry, and immunofluorescent assay

Liver tissue was fixed in z-Fix solution or embedded in Tissue-Tek OCT compound (Sakura Finetek) for paraffin and frozen block preparation, respectively. Paraffin sections were

stained for F4/80 (ebioscience), CD163 (Bioss), PCNA (Santa Cruz), p21 (Santa Cruz), A6 (DSH) and SOX9 (BD Bioscience). Frozen tissue sections were stained for EpCam (BD Bioscience), NK1.1 (BioLegend), F4/80 (ebioscience), CD163 (Bioss), iNOS (abcam), HNF4a (Santa Cruz) and TUNEL assay according to the manufacturer's procedures (Roche). The images were acquired with an Olympus IX71 microscope and CellSense software. For Oil Red-O staining, frozen sections were fixed with 4% PFA in PBS for 10 minutes at room temperature. Slides were washed twice with 1X PBS and permeabilized with 1X PBST for 5 minutes at room temperature with gentle rocking. Slides were washed three times with 1X PBS for 10 minutes each at room temperature, and stained with Oil Red-O solution (4 g/L ORO powder in 60% isopropanol) at 56 °C for 40 min. Slides were washed twice with 1X PBS and counterstained with Vectshield with DAPI mounting medium (Vector Labs). SA-β-gal staining was performed as previously described (Krizhanovsky et al., 2008).

Biochemical assays and reagents

Immunoblotting and quantitative real-time PCR (qPCR) were performed following standard protocols. The total RNAs in the whole liver or tumors were extracted with Trizol reagents (Cat. No. 15596, Invitrogen) using MagNA Lyser (Roche) and reverse transcribed using a kit (Cat. No. 4374966, Invitrogen). Quantitative real-time PCR was performed with master mix (Cat. No. 600882, Agilent Technologies) using Mx3000P qPCR system (Agilent Technologies). Antibodies against p-STAT1, p-STAT3, p-p38, p38, cleaved caspase-3, p53 and GAPDH were from Cell signaling. SOCS1, SOCS3, MAVS, Bax, Bid and perforin were from Santa Cruz Biotechnology; AFP (R&D) and TLR3 (Abcam).

Isolation of leukocytes from liver

Liver was digested enzymatically with pronase (Roche) and collagenase (Sigma) by *in-situ* perfusion. Non-parenchymal cells were isolated by centrifugation at 50 g for 5 min and were laid on top of a four-density Larcoll gradient. The gradients were centrifuged at 20,000 rpm for 30 min at 25 °C using SW41Ti rotor (Beckman). A pure population of Kupffer cells was recovered from the interface between 8% and 12% Nicodenz, washed and immediately frozen in liquid nitrogen for further analysis. The purity of the Kupffer cell fraction was determined by H&E staining of cytospins preparation and always exceeded 90%.

Flow cytometric analysis

Intrahepatic leukocytes, liver-draining lymphocytes and splenocytes were isolated and subjected to FACS analysis as described previously. The following mAbs were used: CD45 (30-F11), F4/80 (BM8), TCFβ (H57-597), CD4 (RM4-5), CD11c (N418), CD11b (M1/70), NK1.1 (PK136), CD115 (AFS98), CD102 (3C4), CD64 (F4-11), CD206 (MMR), MHCII (M5/114.15.2), CD68 (FA-11), Ly-6C (HK1.4), SiglecF (E50-2440) and IgG isotype controls (all from Biolegend San Diego, CA). Foxp3 (FJK-16) was from eBioscience. Flow cytometric analysis was performed on a LSR Fortessa and analyzed with FlowJo (Tree Star, Ashland, OR, USA).

RNA-seq and bioinformatic data analysis

Total RNAs were extracted using QIAGEN RNeasy columns. Poly(A)-selected, unstranded Illumina libraries were prepared with a modified TruSeq protocol. 0.5X AMpure XP beads were added to the sample library to select for fragments of <400 bp, followed by 1X beads to select for fragments >100 bp. These fragments were then amplified with PCR (15 cycles) and separated by gel electrophoresis (2% agarose). 230 bp DNA fragments were isolated and sequenced on the Illumina HiSeq 2000 (single read and 50 run cycles). Raw reads generated by RNA-seq experiments were mapped to the GRCm38 mouse reference genome using Star program (2.3.0). Expression level of each gene in different conditions was obtained using cuffdiff. Differential expression genes were selected based on q-values (<0.05) and fold change (2). Heatmaps in figures were generated using the "heatmap" package in R.

Depletion of macrophages or NK cells

For macrophage depletion, mice were injected 200 μl clodronate liposome, and depletion of NK cells was achieved by intraperitoneal injection of 600 μg anti-NK1.1 (Clone: PK136, Bio X Cell) 24 hrs before pIC injection, and the effect was evaluated 7 days after pIC injection.

Statistical analysis

Statistical analysis was performed using a two-tailed unpaired Student's t-test. Values are presented as mean ± SEM (* $p < 0.05$, ** $p < 0.01$ and *** $p < 0.001$).

Supplementary Material

Refer to Web version on PubMed Central for supplementary material.

Acknowledgments

References

Bard-Chapeau EA, Li S, Ding J, Zhang SS, Zhu HH, Princen F, Fang DD, Han T, Bailly-Maitre B, Poli V, et al. Ptpn11/Shp2 acts as a tumor suppressor in hepatocellular carcinogenesis. Cancer Cell. 2011; 19:629–639. [PubMed: 21575863]

Barton GM, Medzhitov R. Toll-like receptor signaling pathways. Science. 2003; 300:1524–1525. [PubMed: 12791976]

Brausi M, Witjes JA, Lamm D, Persad R, Palou J, Colombel M, Buckley R, Soloway M, Akaza H, Bohle A. A review of current guidelines and best practice recommendations for the management of nonmuscle invasive bladder cancer by the International Bladder Cancer Group. J Urol. 2011; 186:2158–2167. [PubMed: 22014799]

Das M, Garlick DS, Greiner DL, Davis RJ. The role of JNK in the development of hepatocellular carcinoma. Genes Dev. 2011; 25:634–645. [PubMed: 21406557]

Farazi PA, DePinho RA. Hepatocellular carcinoma pathogenesis: from genes to environment. Nat Rev Cancer. 2006; 6:674–687. [PubMed: 16929323]

Feng GS. Conflicting roles of molecules in hepatocarcinogenesis: paradigm or paradox. Cancer Cell. 2012; 21:150–154. [PubMed: 22340589]

Friedman AA, Letai A, Fisher DE, Flaherty KT. Precision medicine for cancer with next-generation functional diagnostics. Nat Rev Cancer. 2015; 15:747–756. [PubMed: 26536825]

Galicia VA, He L, Dang H, Kanel G, Vendryes C, French BA, Zeng N, Bayan JA, Ding W, Wang KS, et al. Expansion of hepatic tumor progenitor cells in Pten-null mice requires liver injury and is reversed by loss of AKT2. Gastroenterology. 2010; 139:2170–2182. [PubMed: 20837017]

He G, Yu GY, Temkin V, Ogata H, Kuntzen C, Sakurai T, Sieghart W, Peck-Radosavljevic M, Leffert HL, Karin M. Hepatocyte IKKbeta/NF-kappaB inhibits tumor promotion and progression by preventing oxidative stress-driven STAT3 activation. Cancer Cell. 2010; 17:286–297. [PubMed: 20227042]

Horie Y, Suzuki A, Kataoka E, Sasaki T, Hamada K, Sasaki J, Mizuno K, Hasegawa G, Kishimoto H, Iizuka M, et al. Hepatocyte-specific Pten deficiency results in steatohepatitis and hepatocellular carcinomas. J Clin Invest. 2004; 113:1774–1783. [PubMed: 15199412]

Krizhanovsky V, Yon M, Dickins RA, Hearn S, Simon J, Miething C, Yee H, Zender L, Lowe SW. Senescence of activated stellate cells limits liver fibrosis. Cell. 2008; 134:657–667. [PubMed: 18724938]

Kuhn R, Schwenk F, Aguet M, Rajewsky K. Inducible gene targeting in mice. Science. 1995; 269:1427–1429. [PubMed: 7660125]

Lanaya H, Natarajan A, Komposch K, Li L, Amberg N, Chen L, Wculek SK, Hammer M, Zenz R, Peck-Radosavljevic M, et al. EGFR has a tumour-promoting role in liver macrophages during hepatocellular carcinoma formation. Nat Cell Biol. 2014; 16:972–981. 971–977. [PubMed: 25173978]

Li S, Hsu DD, Li B, Luo X, Alderson N, Qiao L, Ma L, Zhu HH, He Z, Suino-Powell K, et al. Cytoplasmic Tyrosine Phosphatase Shp2 Coordinates Hepatic Regulation of Bile Acid and FGF15/19 Signaling to Repress Bile Acid Synthesis. Cell Metab. 2014; 20:320–332. [PubMed: 24981838]

Liu C, Liu L, Chen X, Cheng J, Zhang H, Shen J, Shan J, Xu Y, Yang Z, Lai M, Qian C. Sox9 regulates self-renewal and tumorigenicity by promoting symmetrical cell division of cancer stem cells in hepatocellular carcinoma. Hepatology. 2016; 64:117–129. [PubMed: 26910875]

Llovet JM, Zucman-Rossi J, Pikarsky E, Sangro B, Schwartz M, Sherman M, Gores G. Hepatocellular carcinoma. Nat Rev Dis Primers. 2016; 2:16018. [PubMed: 27158749]

Luo X, Liao R, Hanley KL, Zhu HH, Malo KN, Hernandez C, Wei X, Varki NM, Alderson N, Chu C, et al. Dual Shp2 and Pten Deficiencies Promote Non-alcoholic Steatohepatitis and Genesis of Liver Tumor-Initiating Cells. Cell Rep. 2016; 17:2979–2993. [PubMed: 27974211]

Maeda S, Kamata H, Luo JL, Leffert H, Karin M. IKKbeta couples hepatocyte death to cytokine-driven compensatory proliferation that promotes chemical hepatocarcinogenesis. Cell. 2005; 121:977–990. [PubMed: 15989949]

Michelotti GA, Machado MV, Diehl AM. NAFLD, NASH and liver cancer. Nat Rev Gastroenterol Hepatol. 2013; 10:656–665. [PubMed: 24080776]

Mills CD. M1 and M2 Macrophages: Oracles of Health and Disease. Crit Rev Immunol. 2012; 32:463–488. [PubMed: 23428224]

Narayan R, Nguyen H, Bentow JJ, Moy L, Lee DK, Greger S, Haskell J, Vanchinathan V, Chang PL, Tsui S, et al. Immunomodulation by imiquimod in patients with high-risk primary melanoma. J Invest Dermatol. 2012; 132:163–169. [PubMed: 21850019]

Poon RT. Prevention of recurrence after resection of hepatocellular carcinoma: a daunting challenge. Hepatology. 2011; 54:757–759. [PubMed: 21793027]

Ryerson AB, Eheman CR, Altekruse SF, Ward JW, Jemal A, Sherman RL, Henley SJ, Holtzman D, Lake A, Noone AM, et al. Annual Report to the Nation on the Status of Cancer, 1975–2012, featuring the increasing incidence of liver cancer. Cancer. 2016; 122:1312–1337. [PubMed: 26959385]

Song MS, Salmena L, Pandolfi PP. The functions and regulation of the PTEN tumour suppressor. Nat Rev Mol Cell Biol. 2012; 13:283–296. [PubMed: 22473468]

Vargas AJ, Harris CC. Biomarker development in the precision medicine era: lung cancer as a case study. Nat Rev Cancer. 2016; 16:525–537. [PubMed: 27388699]

Wang J, Kubes P. A Reservoir of Mature Cavity Macrophages that Can Rapidly Invade Visceral Organs to Affect Tissue Repair. Cell. 2016; 165:668–678. [PubMed: 27062926]

Wang Q, Yu WN, Chen X, Peng XD, Jeon SM, Birnbaum MJ, Guzman G, Hay N. Spontaneous Hepatocellular Carcinoma after the Combined Deletion of Akt Isoforms. Cancer Cell. 2016; 29:523–535. [PubMed: 26996309]

Wolf MJ, Adili A, Piotrowitz K, Abdullah Z, Boege Y, Stemmer K, Ringelhan M, Simonavicius N, Egger M, Wohlleber D, et al. Metabolic activation of intrahepatic CD8+ T cells and NKT cells causes nonalcoholic steatohepatitis and liver cancer via crosstalk with hepatocytes. Cancer Cell. 2014; 26:549–564. [PubMed: 25314080]

Worby CA, Dixon JE. Pten. Annu Rev Biochem. 2014; 83:641–669. [PubMed: 24905788]

Xu X, So JS, Park JG, Lee AH. Transcriptional control of hepatic lipid metabolism by SREBP and ChREBP. Seminars in liver disease. 2013; 33:301–311. [PubMed: 24222088]

Yamashita T, Wang XW. Cancer stem cells in the development of liver cancer. J Clin Invest. 2013; 123:1911–1918. [PubMed: 23635789]

Zhu HH, Ji K, Alderson N, He Z, Li S, Liu W, Zhang DE, Li L, Feng GS. Kit-Shp2-Kit signaling acts to maintain a functional hematopoietic stem and progenitor cell pool. Blood. 2011; 117:5350–5361. [PubMed: 21450902]

Zou W, Wolchok JD, Chen L. PD-L1 (B7-H1) and PD-1 pathway blockade for cancer therapy: Mechanisms, response biomarkers, and combinations. Sci Transl Med. 2016; 8:328rv324.

Zucman-Rossi J, Villanueva A, Nault JC, Llovet JM. Genetic Landscape and Biomarkers of Hepatocellular Carcinoma. Gastroenterology. 2015; 149:1226–1239. e1224. [PubMed: 26099527]
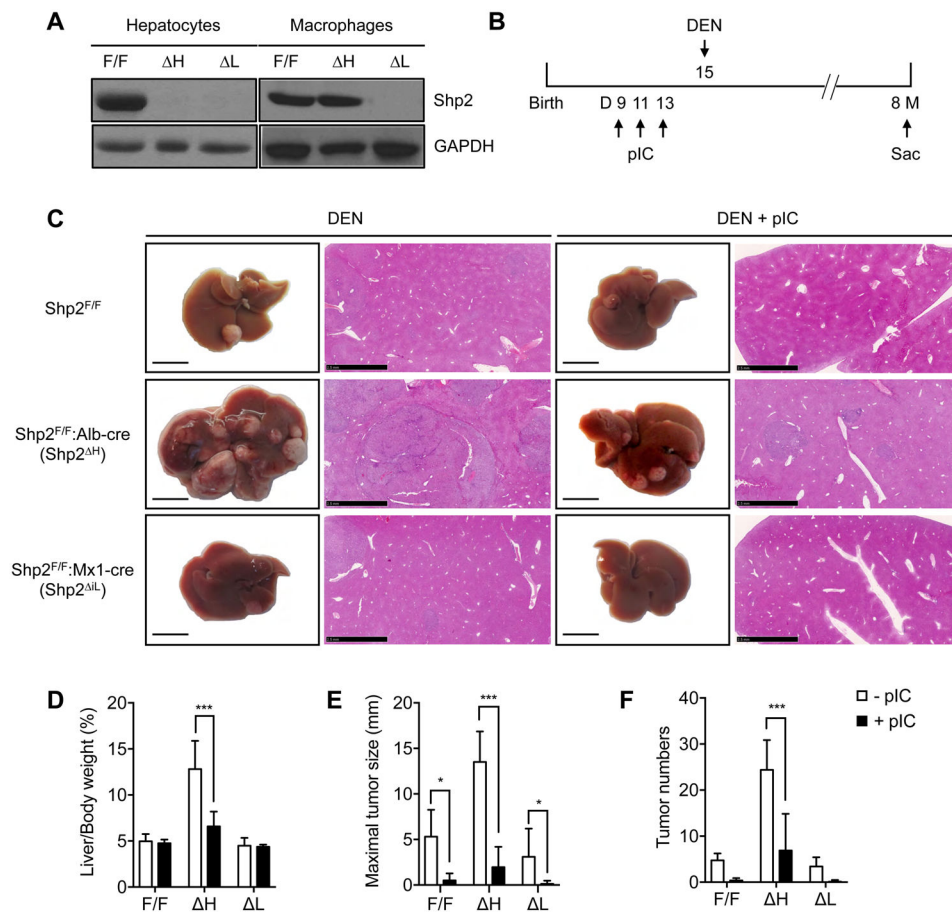
Figure 1. pIC potently inhibits DEN-induced HCC independent of cell type-specific gene deletion in the liver

A. Immunoblotting was performed to determine Shp2 expression in isolated hepatocytes or macrophages in 20-day-old mouse livers.

B, A scheme of experimental procedure for i.p. injection of pIC (15 μg/g) on postnatal day 9, 11, and 13, and then DEN (25 mg/kg of body weight, BW) injection on day 15, into *Shp2^{F/F}*, *Shp2^{F/F}:Alb-cre* (*Shp2^{ΔH}*), and *Shp2^{F/F}:Mx1-cre* (*Shp2^{ΔiL}*) mice.

C, Representative livers of 8-month-old DEN-treated male mice with or without pIC injection (scale bar, 1 cm), and H&E staining of liver sections of indicated genotypes. Scale bars: 2.5 mm. Objective magnification: ×1.25.

D, Calculated percentages of liver/body weights.

E, Maximal tumor sizes (diameters) were measure.

F, The numbers of tumor nodules were counted on liver surface. The data in (**D–F**) are shown as means ± S.E., n = 12, * p < 0.05 and *** p < 0.0001, by Student's t-test.

F/F: floxed mice;   ΔH: gene deleted in hepatocytes;   ΔiL: gene deletion in hepatocytes and non-parenchymal cells was induced by pIC injection.
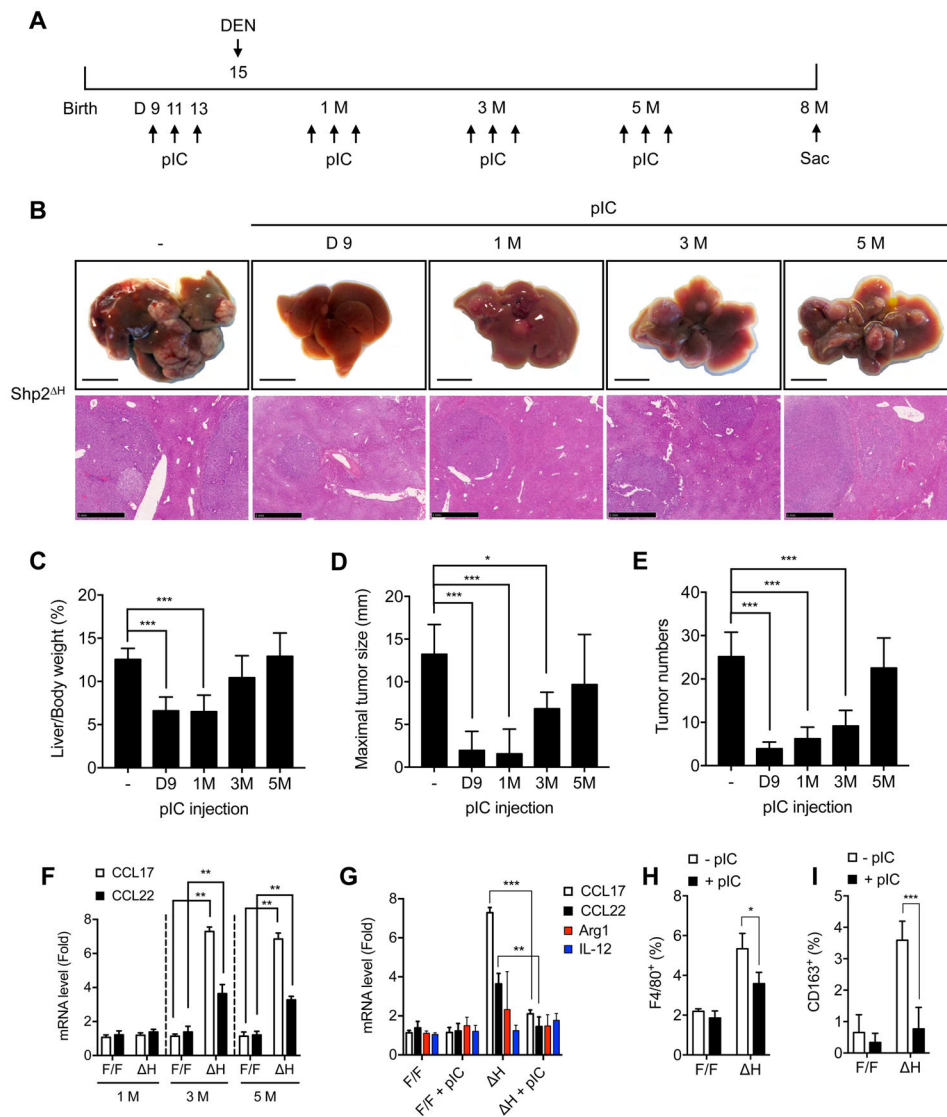
Figure 2. pIC has preventive effect in hepatocarcinogenesis in the early stages

A, A scheme of experimental procedure using *Shp2*^{H} (*Shp2*$^{F/F}$:*Alb-cre*) mice. All mice received DEN (25 mg/kg of BW) on day 15, and pIC (15 μg/g) was given on day 9, or 1, 3, 5 months of age with 3 i.p. injections every other day. All mice were sacrificed at 8 months.

B, Representative livers of 8-month-old DEN-treated male mice (scale bar: 1 cm) and H&E staining of liver sections of indicated genotypes (scale bars: 1 mm; objective magnification: ×2.5).

C, Calculated percentages of liver versus body weights.

D, Maximal tumor sizes (diameters).

E, The numbers of tumor nodules on liver surface.

The data in (**C**–**E**) are shown as means ± S.E. *n* = 6, * p < 0.05 and *** p < 0.0001, Student t-test.

F, *Shp2*$^{F/F}$ and *Shp2*^{H} mice were given DEN on day 15, and hepatic expression of CCL17 and CCL22 was examined at 1, 3, 5 months using qRT-PCR.

G, The expression of M2-related genes (CCL17, CCL22 and Arginase 1) or M1-related gene (IL-12) was examined in livers of 3-month-old *Shp2*$^{F/F}$ and *Shp2*^{H} mice that received DEN on day 15 and were treated with or without pIC on day 9, 11, and 13 ($n = 5$).

H–I, Quantification for IHC staining of F4/80 and CD163 in 3-month-old *Shp2*$^{F/F}$ and *Shp2*^{H} livers. qPCR data are shown as means ± S.E. * p < 0.05, ** p < 0.001, *** p < 0.0001, Student t-test.
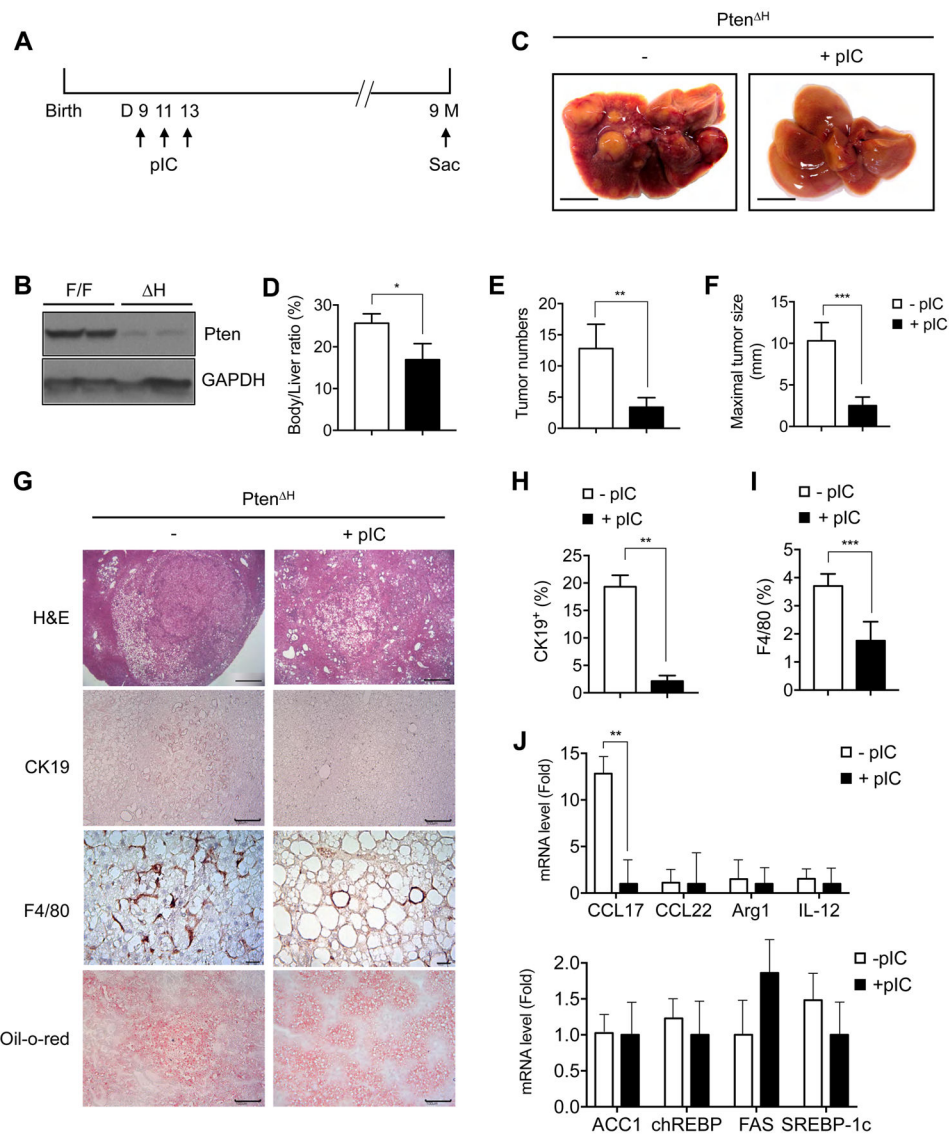
Figure 3. Inhibitory effect of pIC on liver tumorigenesis driven by Pten deficiency and hepatosteatosis

A, *Pten*[ΔH] mice received pIC (15 μg/g) on day 9, 11, 13, and were sacrificed to examine tumor loads at 9 months.

B, Immunoblotting of *Pten* expression in liver lysates of control (*Pten*[F/F]) and *Pten*[ΔH] (*Pten*[F/F]:*Alb-cre*) mice.

C, Representative livers of 9-month-old *Pten*[ΔH] mice with or without pIC injection.

D, The percentages of liver versus body weights.

E, The numbers of tumor nodules on liver surface.

F, Maximal tumor sizes in diameters.

G, H&E, Oil-o-red, or immunostaining for CK19 (cholangiocytes) and F4/80 (macrophages) of liver sections as indicated (Scale bar: 100 μm).

H, I, Quantification of CK19^{+} and F4/80[+] areas was performed from images in (**G**).

J, qRT-PCR was performed to determine expression of M2-related or lipogenic genes in 9-month-old *Pten* ^{H} livers. The data are shown as means ± S.E. ($n = 6$; * p < 0.05, ** p < 0.001; *** p < 0.0001, Student t-test).
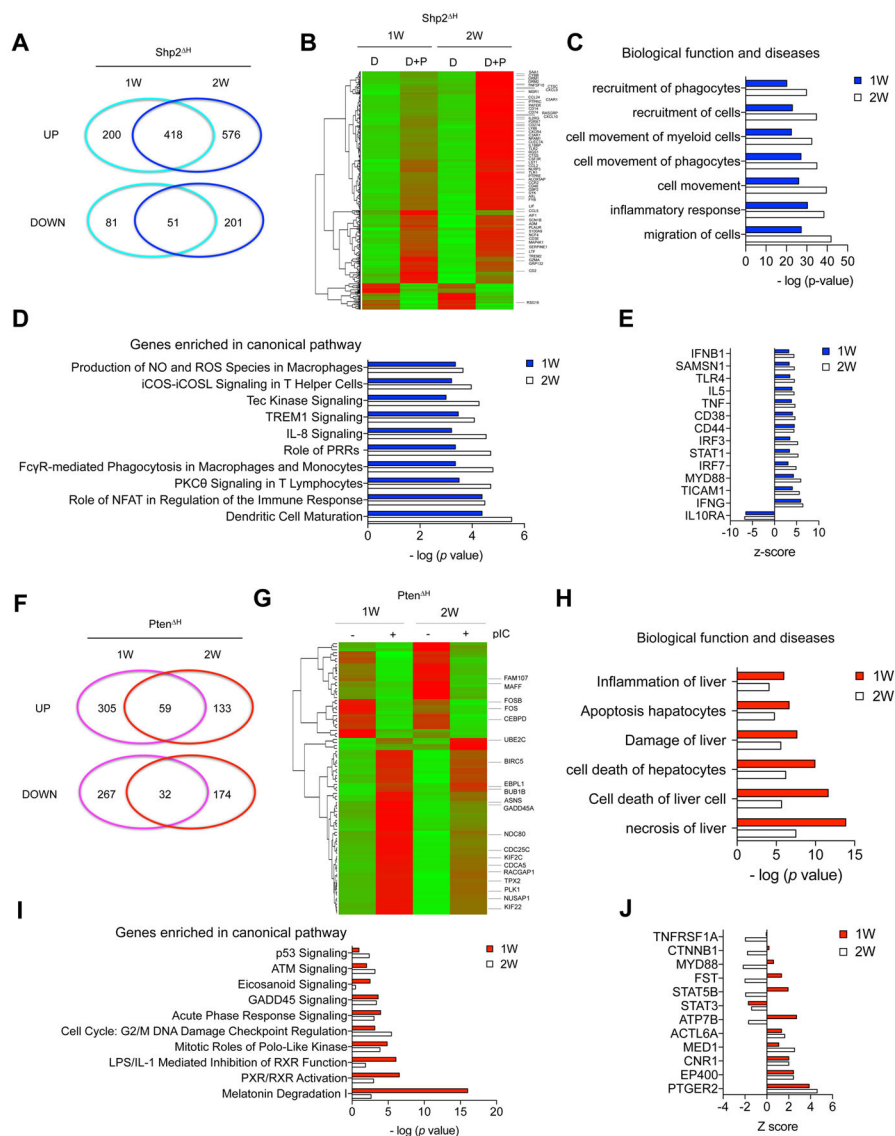
Figure 4. Comprehensive analysis of gene expression profiles modulated by pIC in Shp2 [H] or Pten [H] mice

Shp2 [H] mice received pIC on D9, 11, 13, and DEN on D15. Total RNAs were extracted from control or pIC-treated livers 7 or 14 days after the last pIC injection for RNA-seq analysis.

Pten [H] mice were treated with or without pIC in the same way, without receiving DEN, and total RNAs were extracted 1 or 2 weeks for RNA-seq analysis ($n = 3$).

A, Venn diagram shows the numbers of up- or down-regulated genes at 7 and 14 days after pIC injection in *Shp2* [H] livers.

B, Heatmap of the 418 up- and 51 down-regulated genes that were shared at 1 and 2 weeks in pIC-treated *Shp2* [H] livers. Highlights of genes related to immune response.

C, pIC-modulated genes were mainly involved in immune cell functions by IPA.

D, The top 10 canonical pathways altered by pIC were identified in *Shp2* [H] livers by IPA analysis. Dendritic cell maturation; Role of nuclear factor of activated T-cells (NFAT) in

regulation of immune response, protein kinase C (PKC) signaling in T cells, Fc-receptor phagocytosis in macrophage and monocytes, Role of pattern recognition receptors; IL-8 signaling; The triggering receptor expressed on myeloid cells 1 (TREM1) signaling; Tec Kinase signaling; inducible costimulator (iCOS)-iCOS ligand (iCOSL) signaling in Th cells; production of nitric oxide (NO) and reactive oxygen species (ROS) in macrophages.

E, Predicted activation/inhibition of upstream factors done by IPA based on differentially expressed genes.

F, Venn diagram shows the numbers of commonly or distinctly changed genes at 7 and 14 days in pIC-treated *Pten* ^{H} livers.

G, Heatmap shows the commonly changed genes (59 up and 32 down) mainly involved in cell cycle and apoptosis in *Pten* ^{H} livers. Highlights of genes involved in cell cycle and apoptosis.

H, pIC-modulated genes were enriched in apoptosis/cell death pathways and suppression of tumor growth by IPA.

I, Top 10 pathways in pIC-treated *Pten* ^{H} livers using IPA analysis.

J, Predicted activation/inhibition of upstream factors based on differentially expressed genes analyzed by IPA.
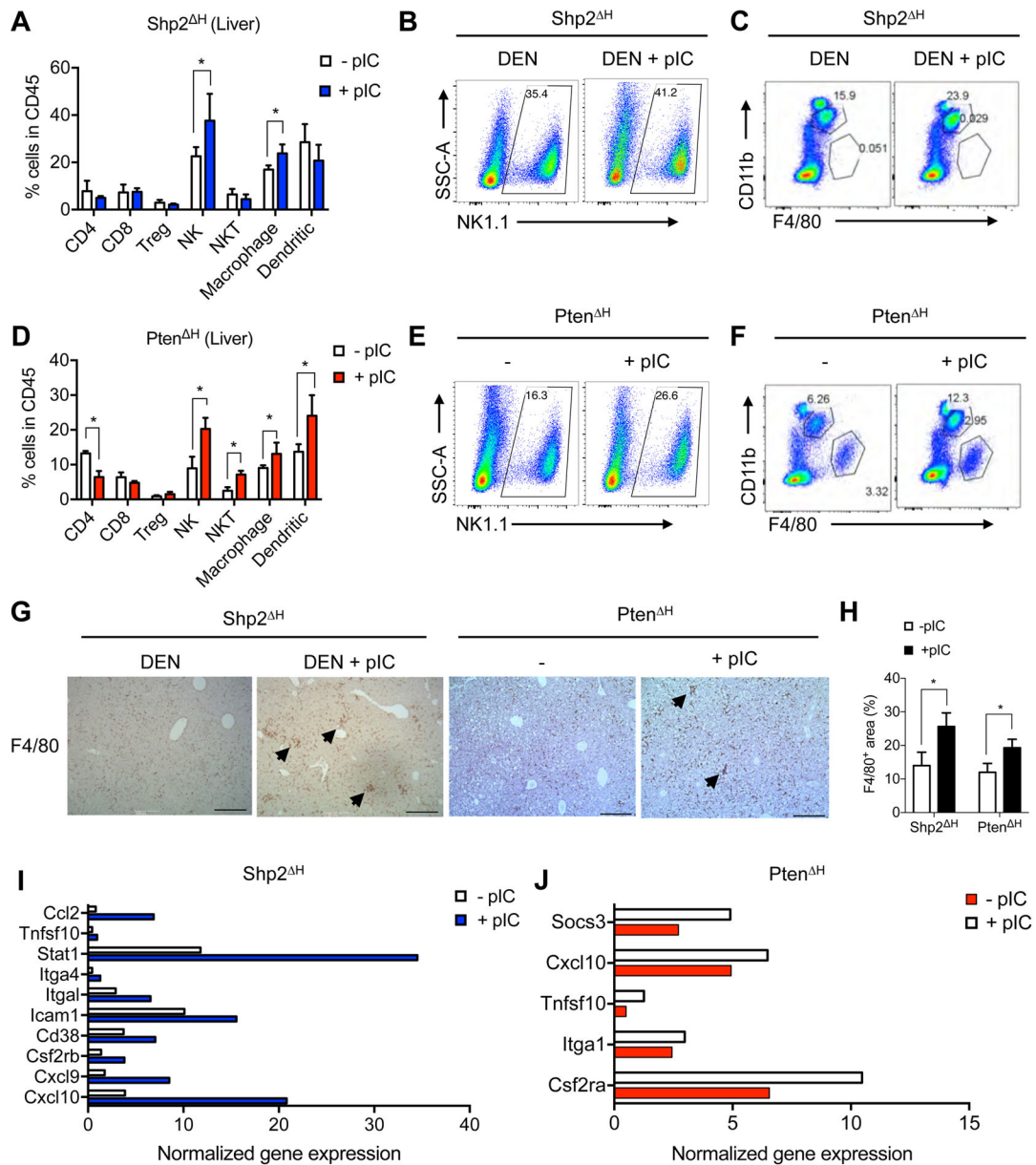
Figure 5. Regulation of innate immunity by pIC

Flow cytometry analysis was performed for immune cell subsets in whole livers of *Pten*^H and DEN-treated *Shp2*^H mice 7 days after pIC injection, in accordance with the RNA-seq analysis.

A, FACS of immune cell subsets in whole livers of *Shp2*^H mice.

B, NK1.1+ NK cells examined in *Shp2*^H livers.

C, Macrophages (CD11b+ F4/80+) analyzed in *Shp2*^H livers.

D, FACS of immune cell subsets in whole livers of *Pten*^H mice.

E, NK1.1+ NK cells in *Pten*^H livers.

F, Macrophages (CD11b+ F4/80+) in *Pten*^H livers.

G, Immunostaining for F4/80+ cells in *Shp2*^H and *Pten*^H livers (Scale bar: 100 μm).

H, F4/80$^+$ areas were quantified from images shown in (G) ($n = 6$).

I, J, GSEA identified pIC-induced expression profiles of M1 macrophage-related genes and NK cell activation genes in *Shp2* ^{H} and *Pten* ^{H} livers.

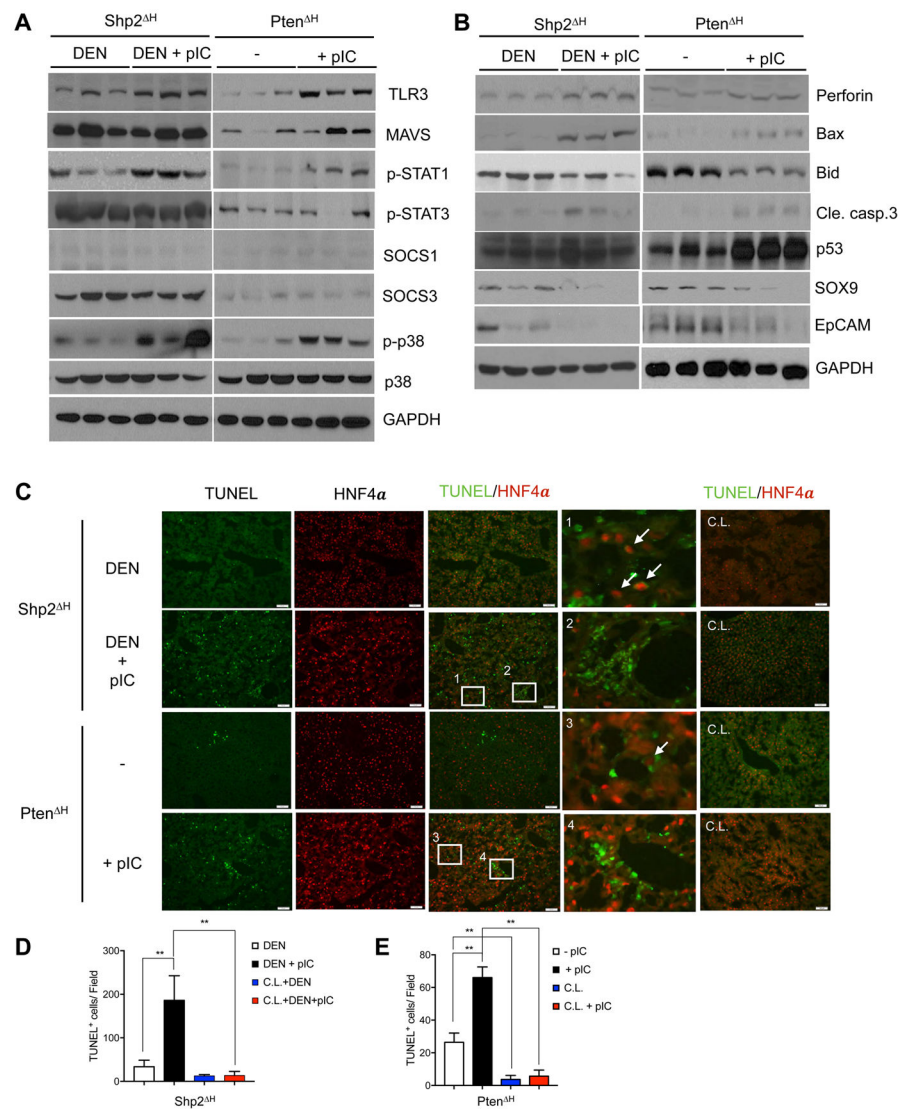Data are shown as means ± S.E. * p < 0.05, Student t-test.

Figure 6. pIC modulates multiple signaling pathways and hepatic responses in Shp2^ΔH and Pten^ΔH mice

A, B, Immunoblotting of liver lysates prepared at 1 week after pIC injection into *Pten^ΔH* or DEN-treated *Shp2^ΔH* mice, to determine the protein or phospho-protein amounts as indicated. Focuses were on the molecules involved in the TLR3 pathway, cell death and TIC biomarkers.

C. Representative images of for co-staining of TUNEL signals and HNF4α performed on liver sections 7 days after pIC injection, with white arrows indicating TUNEL^+ cells merged with HNF4α. Clodronate liposome (C.L.) was injected for macrophage depletion model 24 hrs before pIC treatment.

D, TUNEL^+ cells were quantified from images shown in Figure 7C in DEN-treated *Shp2^ΔH* mice.

E, TUNEL^+ cells were quantified from images shown in Figure 7C after macrophage in *Pten^ΔH* mice. ($n = 5$; * p< 0.05, Student t-test).
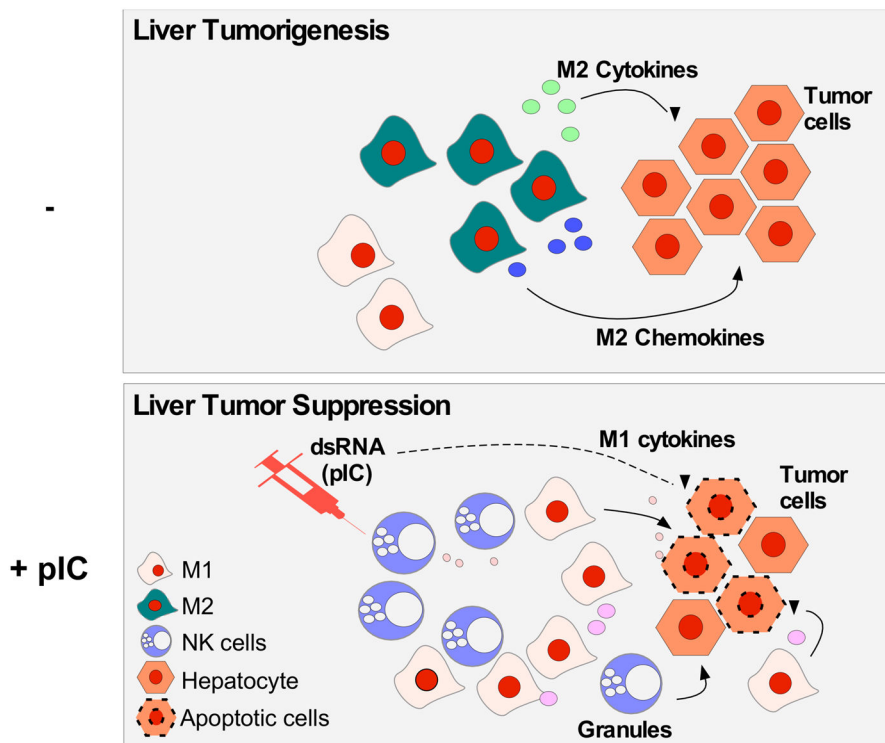
Figure 7. A model for pIC-mediated inhibition of liver tumorigenesis
The inhibitory effect of pIC on liver cancer initiation is likely through systemic activation of multiple innate immune functions involving activating NK cells, reprogramming M1 and M2 macrophages, promoting injured hepatocyte death and suppressing tumor cell genesis and expansion.